Article

Discovery Medicine 2025; 37(201): 2214–2223
https://doi.org/10.24976/Discov.Med.202537201.188

Angelicin Mitigating Renal Fibrosis and Treating IgA Nephropathy via the ESR1-FOS Pathway

Hejing Fang[1,*,†], Ling Zhou[2,†], Xuchun Xu[1], Tingting Zhang[1], Shuangqing Li[1], Can Jin[1]

[1]Department of Nephrology, Jinhua Municipal Central Hospital, 32100 Jinhua, Zhejiang, China
[2]Department of Radiotherapy, Jinhua Municipal Central Hospital, 32100 Jinhua, Zhejiang, China
*Correspondence: fhj602@163.com (Hejing Fang)
[†]These authors contributed equally.
Submitted: 27 June 2025 Revised: 12 August 2025 Accepted: 25 August 2025 Published: 20 October 2025

Background: Immunoglobulin A nephropathy (IgAN) is a common primary glomerular disease characterized by the deposition of IgA or its complexes in the renal mesangium. Despite the availability of medications for treating IgAN, finding more effective treatment methods remains a critical need. Angelicin has shown potential therapeutic effects on IgAN due to its unique anti-inflammatory and antioxidative properties.

Methods: Immunofluorescence, Western blotting and enzyme-linked immunosorbent assay (ELISA) approaches were employed to investigate the therapeutic efficacy of angelicin in a rat model with IgAN. The hTFtarget database was used to predict estrogen receptor 1 (ESR1) targets, while analysis of the GSE35489 dataset through the Gene Expression Omnibus (GEO) database was conducted to identify the role of Fos proto-oncogene (FOS) in fibrosis regulation.

Results: Treatment with angelicin significantly reduced IgA deposition, improved kidney tissue structure, decreased the rate of cell apoptosis, alleviated renal fibrosis ($p < 0.01$), and suppressed the expression of inflammation markers interleukin (IL)-1β, IL-6, and IL-18 ($p < 0.001$). Moreover, the expression of ESR1, FOS, phosphorylated c-Jun (p-c-Jun) and phosphorylated mitogen-activated protein kinase (p-MAPK) was downregulated by angelicin in a dose-dependent manner ($p < 0.05$).

Conclusions: Angelicin can effectively mitigate renal fibrosis and inflammation in IgAN via the ESR1-FOS signaling pathway, highlighting its potential as a viable therapeutic agent for IgAN. This discovery provides new molecular targets and a theoretical basis for the pharmacological treatment of IgAN.

Keywords: angelicin; IgA nephropathy; renal fibrosis; estrogen receptor 1-Fos proto-oncogene pathway

Introduction

Immunoglobulin A nephropathy (IgAN), as the most prevalent form of primary glomerulonephritis worldwide, poses significant challenges within chronic kidney disease (CKD) management, particularly as it often progresses to end-stage renal disease [1,2]. IgAN is an immune complex-mediated glomerular disease in which IgA or IgA-dominant immune complexes are deposited in the glomerular tunica albuginea region, causing inflammatory changes in the glomerulus and leading to varying degrees of renal damage [3,4]. Despite advances in targeted therapies—such as sibeprenlimab, which has demonstrated significant efficacy in reducing proteinuria (NCT04287985)—the complex pathogenesis of IgAN, involving both immune system dysregulation and genetic factors, continues to pose substantial challenges to effective treatment [5]. The disorder's resistance to conventional treatments necessitates ongoing research into more effective therapies, including novel pharmacological agents and integrative medicine approaches [6,7].

Angelicin, a potent furanocoumarin extracted from lalang grass rhizome, has garnered significant attention in the pharmacological research on renal diseases due to its distinct anti-inflammatory and anti-fibrotic properties [8–10]. These attributes are particularly valuable in the context of IgAN, where pathological changes in the kidney are closely associated with inflammation-driven fibrosis. Based on the predicted targets of *Angelica sinensis* identified using Bioinformatics Analysis Tool for Molecular Mechanism of Traditional Chinese Medicine (BATMAN-TCM), we found that the estrogen receptor 1 (*ESR1*) gene may be involved in IgAN development [11]. Recent studies have indicated that angelicin can modulate the activity of key transcription factors such as ESR1 and Fos proto-oncogene (FOS), which play pivotal roles in the signaling pathways governing cellular growth, differentiation, and fibrotic responses [12–14]. Therefore, ESR1 and FOS were selected as the key molecular targets for verifying the mechanism of action of angelicin in this study. We thus hypothesized that angelicin ameliorates IgAN by dual modulation of ESR1 and FOS signaling.

This study aims to explore the effect of angelicin on renal dysfunction and inflammatory response in IgAN models and to delineate the related molecular mechanisms. In the present study, we systematically assessed the therapeutic effects of angelicin on a rat model of IgAN, with a particular focus on its ability to alleviate renal dysfunction and pathological changes in the kidneys.

Materials and Methods

Experimental Design

Male Sprague–Dawley rats (8 weeks old) were procured from the Hangzhou Medical College (Hangzhou, China), each weighing between 200 and 230 g. Prior to treatments, the rats were acclimatized under standard laboratory conditions for seven days, with free access to food and water. The rats were housed under standard conditions with a 12-hour light/dark cycle, at a temperature of 22 °C and humidity of 55%. The rats were randomly divided into five groups (n = 10 per group): a healthy control group (Con), an IgAN model group (IgAN), and three treatment groups receiving 20 mg/kg, 40 mg/kg, and 60 mg/kg of angelicin [15,16] (523-50-2, Sigma-Aldrich, St. Louis, MO, USA), respectively.

IgAN Model Establishment and Treatment

The IgAN model was established by intravenous injection of 1 mg/day bovine γ-globulin (BGG; 23212, Thermo Fisher Scientific, Waltham, MA, USA) into the rats' tail veins for three consecutive days [17]. Following the initial phase, the rats were orally administered 0.1% BGG mixed with 6 mM HCl in tap water for eight consecutive weeks. The rats in the control group did not receive any treatment during the experiment. Each treatment group received daily gastric infusions of angelicin at doses of 20/40/60 mg/kg from week 9 to week 12 [15,16]. All surgical procedures were performed on rats already anesthetized with 4% isoflurane (26675-46-7, Sigma-Aldrich, St. Louis, MO, USA). At the end of the experiment, all animals were sacrificed by an intraperitoneal injection of 2% pentobarbital sodium (100 mg/kg). To ensure accuracy, all rats were fasted for 12 hours prior to execution. All samples were collected at week 12 during the study period. Animal carcasses were collected and disposed of by Hangzhou DaDi Environmental Protection Co., in accordance with relevant biosafety and environmental regulations.

Rat Weight Measurement

Body weight of the rats, a crucial indicator of their health status, was measured before euthanasia. All rat weights were recorded during the same time frame (9:00 AM to 10:00 AM) using an electronic scale to ensure data consistency and comparability. Six biological replicates were performed for each group.

Urine Protein Measurement

Urine samples of the rats were collected at week 12, over a 24-hour period. To prevent sample contamination, specially designed metabolic cages that allow for the separation of urine and feces were utilized. The collected urine samples were preserved in centrifuge tubes containing preservatives at 2–8 °C to prevent protein degradation. Protein levels were quantified using the Bradford Assay Kit (ab102535, Abcam, Cambridge, UK), following the manufacturer's instructions. Six biological replicates were performed for each group.

Serum Creatinine and Urea Nitrogen Measurement

Blood samples of the rats were collected at the end of the study. All rats were fasted for 12 hours prior to sampling. Two milliliters of blood were drawn into sterile disposable tubes from each rat's tail vein under 4% isoflurane gas anesthesia. Serum creatinine and urea nitrogen concentrations were determined using an automated biochemical analyzer (98640000, Thermo Fisher Scientific, Waltham, MA, USA). Six biological replicates were performed for each group.

Glomerular Filtration Rate Measurement

Glomerular filtration rate (GFR) was measured using the creatinine clearance method [18]. Catheterization was performed in the carotid artery, bladder, and tail vein of the rats anesthetized with 4% isoflurane gas. A physiological saline solution containing creatinine (F3272, Sigma-Aldrich, St. Louis, MO, USA) was administered intravenously, starting with a 0.5 mL injection of 1% creatinine solution followed by a continuous infusion at 2 mL/hour. After a stabilization period of at least 60 minutes, urine samples were collected hourly. In the middle of each urine collection period, approximately 400 µL of blood was collected from the carotid artery to measure blood creatinine levels. GFR was calculated based on the ratio of creatinine in urine to that in blood. Six biological replicates were performed for each group.

Enzyme-Linked Immunosorbent Assay for Measuring Glycosylated IgA1 Levels

For this experiment, a sandwich enzyme-linked immunosorbent assay (ELISA) for glycosylated IgA1 (Gd-IgA1) was constructed using a specific antibody against Gd-IgA1 (10777, IBL, Fujisawa, Japan) [19,20]. The specific Gd-IgA1 antibody (at a concentration of 7.5 µg/mL) was diluted with phosphate-buffered saline (PBS) and then coated onto an ELISA plate (NUNC MaxiSorp; Thermo Fisher Scientific, Waltham, MA, USA). The plate was then incubated at room temperature for 18 hours. Afterward, 50 µL of the blood sample was added to each well, and this was followed by a 2-hour incubation at room temperature. Following washing, a 1000× diluted HRP-labeled rabbit monoclonal antibody (ab193187, Abcam, Cambridge, UK)

against human IgA1 α1-chain was incubated at room temperature for 2 hours. After washing, color development was performed using SIGMAFAST o-phenylenediamine (OPD) solution (P9187, Sigma-Aldrich, St. Louis, MO, USA), and the reaction was terminated by adding 1 M sulfuric acid (127062-22-0, Sigma-Aldrich, St. Louis, MO, USA). The absorbance was recorded at 490 nm, and the level of Gd-IgA1 was determined by reference to a standard curve (4-parameter logistic curve fitting) and expressed in units. In this study, 1 unit was defined as 1 ng/mL of standard Gd-IgA1. Six biological replicates were performed for each group.

Immunofluorescence

The renal tissues obtained from the rats were rapidly frozen at –20 °C and then sectioned into 5-µm-thick slices using a cryostat. The sections were then mounted on glass slides and allowed to air dry. After drying, the sections were fixed and then incubated with PBS containing 1% bovine serum albumin (9048-46-8, Sigma-Aldrich, St. Louis, MO, USA). Following this blocking step, the sections were incubated overnight at 4 °C with a 10× diluted solution of Texas Red Polyclonal rabbit anti-IgA antibody (32460, Thermo Fisher Scientific, Waltham, MA, USA). After incubation, the sections were washed and stained with 4′,6-diamidino-2-phenylindole (DAPI, 28718-90-3, Sigma-Aldrich, St. Louis, MO, USA) and then coverslipped. The stained sections were observed at a magnification of 600× and photographed with a scale bar representing 50 µm using a fluorescence microscope (Carl Zeiss AG, Zeiss LSM 900, Jena, Germany). Three biological replicates were performed for each group.

Histological Processing and Hematoxylin & Eosin (H&E) Staining

Renal tissues were promptly collected from euthanized rats and fixed in 10% neutral buffered formalin (E672001-0001, Sangon Biotech, Shanghai, China). After fixation, the tissues underwent dehydration and clearing in gradient alcohol solutions and xylene (A530011-0500, Sangon Biotech, Shanghai, China), respectively, before being embedded in paraffin (A601801-0500, Sangon Biotech, Shanghai, China). Tissue sections, each 3-µm-thick, were cut and stained using H&E (E607318, Sangon Biotech, Shanghai, China). Stained sections were observed under a microscope (Axio Lab.A1, Carl Zeiss, Oberkochen, Germany) at a magnification of 100× and photographed with a scale bar representing 100 µm. Three biological replicates were performed for each group.

Terminal Deoxynucleotidyl Transferase Mediated dUTP Nick-end Labeling Assay

Kidney tissues were fixed in 10% neutral buffered formalin, followed by dehydration and clearing. The tissues were then embedded in paraffin and sectioned into 5-µm-thick slices. The sections were dewaxed in xylene and rehydrated in a series of ethanol solutions of decreasing concentrations. Before staining with a commercial terminal deoxynucleotidyl transferase mediated dUTP nick end labeling (TUNEL) kit (E607172-001, Sangon Biotech, Shanghai, China), the sections were treated with proteinase K (A610451-0050, Sangon Biotech, Shanghai, China) and incubated at 37 °C for 60 minutes. After staining, the sections were developed using 3,3′-diaminobenzidine (DAB) (A690009, Sangon Biotech, Shanghai, China) and then counterstained with hematoxylin (E607317-0100, Sangon Biotech, Shanghai, China). TUNEL-positive cells were visualized at a magnification of 100× and photographed at a scale bar representing 100 µm using a fluorescence microscope (Carl Zeiss AG, Zeiss LSM 900, Jena, Germany). Three biological replicates were performed for each group.

Masson Trichrome Staining

Kidney tissues were fixed in 10% neutral buffered formalin, followed by dehydration and clearing. The tissues were then embedded in paraffin and sectioned into 4-µm-thick slices. The sections were dewaxed in xylene, rehydrated through a series of ethanol solutions, and stained using the Masson Trichrome kit (HT15-1KT; Sigma, St. Louis, MO, USA) in accordance with the manufacturer's instructions. The stained sections were then observed under a microscope at a magnification of 100× and photographed at a scale bar representing 100 µm. The extent of interstitial fibrosis was quantified using the Image-Pro Plus 6.0 software (Media Cybernetics, Bethesda, MD, USA), which was used to calculate the average percentage of fibrotic area per section. Three biological replicates were performed for each group.

Immunohistochemical Staining of α-Smooth Muscle Actin (α-SMA) and Collagen Type IV (Col-IV)

Kidney tissues were fixed in 10% neutral buffered formalin, followed by dehydration and clearing. The tissues were then embedded in paraffin and sectioned into 4-µm-thick slices. The sections were dewaxed in xylene and rehydrated in ethanol solutions. After blocking endogenous peroxidase activity with 3% hydrogen peroxide (609978, Sigma-Aldrich, St. Louis, MO, USA), the sections were incubated with primary antibodies against α-SMA (0.034 µg/mL, ab7817, Abcam, Cambridge, UK) and Col-IV (1:500, ab217147, Abcam, Cambridge, UK). Subsequently, they were incubated with Goat Anti-Rabbit IgG H&L (ab205718, Abcam, Cambridge, UK) and Goat Anti-Mouse IgG H&L (ab150113, Abcam, Cambridge, UK), developed using DAB substrate, and counterstained with hematoxylin to enhance contrast. The staining results for α-SMA and Col-IV in renal tissues were observed under an optical microscope at a magnification of 100×, photographed at a scale representing 100 µm, and quantitatively analyzed using ImageJ software (National Institutes

of Health, Bethesda, MD, USA). Three biological replicates were performed for each group.

Western Blotting

Protein levels of Transforming growth factor beta 1 (TGF-β1) (44 kDa), Col-IV (161 kDa), fibronectin 1 (232 kDa), ESR1 (66 kDa), FOS (41 kDa), c-Jun (39 kDa), p-c-Jun (42 kDa), MAPK (40 kDa), p-MAPK (42 kDa) and glyceraldehyde-3-phosphate Dehydrogenase (GAPDH, 36 kDa) were assessed by means of Western blotting. Firstly, kidney tissues were lysed in radioimmunoprecipitation assay (RIPA) buffer containing protease and phosphatase inhibitors (89900, Thermo Fisher Scientific, Waltham, MA, USA) to preserve protein integrity. Following lysis, the lysates were centrifuged at 14,000 $\times g$ for 15 minutes at 4 °C, and the supernatant containing the protein extract was collected. Protein concentrations were determined using a bicinchoninic acid (BCA) Protein Assay Kit (23225, Pierce Biotechnology, Rockford, IL, USA). Protein samples were separated by sodium dodecyl sulfate–polyacrylamide gel electrophoresis (SDS-PAGE). Upon transferring onto polyvinylidene difluoride (PVDF) membranes, the separated protein bands were probed with specific primary antibodies against TGF-β1 (ab215715, Abcam, Cambridge, UK), Col-IV (ab6586, Abcam, Cambridge, UK), fibronectin 1 (ab2413, Abcam, Cambridge, UK), ESR1 (ab79413, Abcam, Cambridge, UK), FOS (ab208942, Abcam, Cambridge, UK), c-Jun (ab40766, Abcam, Cambridge, UK), p-c-Jun (ab32385, Abcam, Cambridge, UK), MAPK (#9212, Cell Signaling Technology, Danvers, MA, USA), p-MAPK (#9101, Cell Signaling Technology, Danvers, MA, USA) and GAPDH (ab8245, Abcam, Cambridge, UK). Following primary antibody incubation, the membranes were washed and incubated with Goat Anti-Mouse IgG H&L (ab150113, Abcam, Cambridge, UK) for FOS and GAPDH, and Goat Anti-Rabbit IgG H&L (ab205718, Abcam, Cambridge, UK) for others, at room temperature for 1 hour. Chemiluminescent detection was performed using an enhanced chemiluminescence (ECL) system (Amersham Pharmacia, Piscataway, NJ, USA) with chemiluminescence reagents from Millipore (Billerica, MA, USA). Three biological replicates were performed for each group.

ELISA for Interleukin (IL)-1β, IL-6 and IL-18 Levels

ELISA kits were used to measure IL-1β (MLB00C, R&D Systems, Minneapolis, MN, USA), IL-6 (M6000B, R&D Systems, Minneapolis, MN, USA) and IL-18 (DL180, R&D Systems, Minneapolis, MN, USA) in the rats' serum samples, according to the manufacturer's instructions. Six biological replicates were performed for each group.

Statistical Analysis

Data were analyzed using GraphPad Prism 8.0 software (GraphPad Software, San Diego, CA, USA). Multiple group comparisons were performed using one-way analysis of variance (ANOVA) followed by Tukey's post hoc test. The Shapiro–Wilk test was used to assess normality of data distribution, and the Brown–Forsythe test was used to verify the homogeneity of variance. Statistical significance was set at $p < 0.05$. Results are expressed as mean $\pm$ standard deviation.

Results

Angelicin Alleviates Renal Dysfunction

To explore the effects of angelicin on renal dysfunction in an IgAN rat model, we first assessed its impact on the rats' body weight. The results showed that various concentrations of angelicin (20/40/60 mg/kg) did not significantly affect the body weight of IgAN rats (Fig. 1A, F = 0.0577, DFn = 4, DFd = 25). In terms of renal function, compared to the control group, IgAN rats exhibited more severe proteinuria (5.04 $\pm$ 0.41 vs. 43.47 $\pm$ 3.76, $p < 0.001$, F = 305.9741, DFn = 4, DFd = 25, Fig. 1B), serum creatinine (0.59 $\pm$ 0.06 vs. 1.04 $\pm$ 3.76, $p < 0.001$, F = 49.3351, DFn = 4, DFd = 25, Fig. 1C), and urea nitrogen (12.15 $\pm$ 1.02 vs. 26.68 $\pm$ 1.85, $p < 0.001$, F = 86.4119, DFn = 4, DFd = 25, Fig. 1D), and a significant decrease in glomerular filtration rate (GFR) (1.59 $\pm$ 0.12 vs. 0.48 $\pm$ 0.05, $p < 0.001$, F = 135.2003, DFn = 4, DFd = 25, Fig. 1E). In a dose-dependent manner, treatment with angelicin significantly reduced these biochemical markers ($p < 0.01$, Fig. 1B–D) and improved GFR ($p < 0.001$, Fig. 1E), with higher doses exerting more significant effects. Additionally, ELISA results indicated that compared to the control group, levels of IgA (6995.57 $\pm$ 65.63 vs. 9999.85 $\pm$ 89.24, $p < 0.001$, F = 1814.8279, DFn = 4, DFd = 25, Fig. 1F) and Gd-IgA1 (6.87 $\pm$ 0.47 vs. 13.42 $\pm$ 0.94, $p < 0.001$, F = 80.0628, DFn = 4, DFd = 25, Fig. 1G) were significantly higher in IgAN rats, but were significantly reduced after treatment with angelicin, with greater reductions observed with increasing doses of the compound ($p < 0.001$, Fig. 1F,G). These experimental results suggest that angelicin can effectively alleviate renal dysfunction caused by IgAN.

Therapeutic Effects of Angelicin on IgAN Rats

A multifaceted analytical approach covering aspects from pathological tissue damage to inflammation marker levels was employed to systematically assess the therapeutic effects of angelicin on the IgAN rat model. First, immunofluorescence staining results revealed significant IgA deposition in the glomeruli of the IgAN group, appearing as granular red fluorescence (100 $\pm$ 8.87 vs. 297.48 $\pm$ 5.59, $p < 0.001$, F = 24.0166, DFn = 4, DFd = 10, Fig. 2A,B). After treatment with angelicin, IgA deposition was significantly reduced (297.48 $\pm$ 5.59 vs. 161.67 $\pm$ 22.39, 110.18 $\pm$ 41.14, $p < 0.01$, Fig. 2A,B), indicating

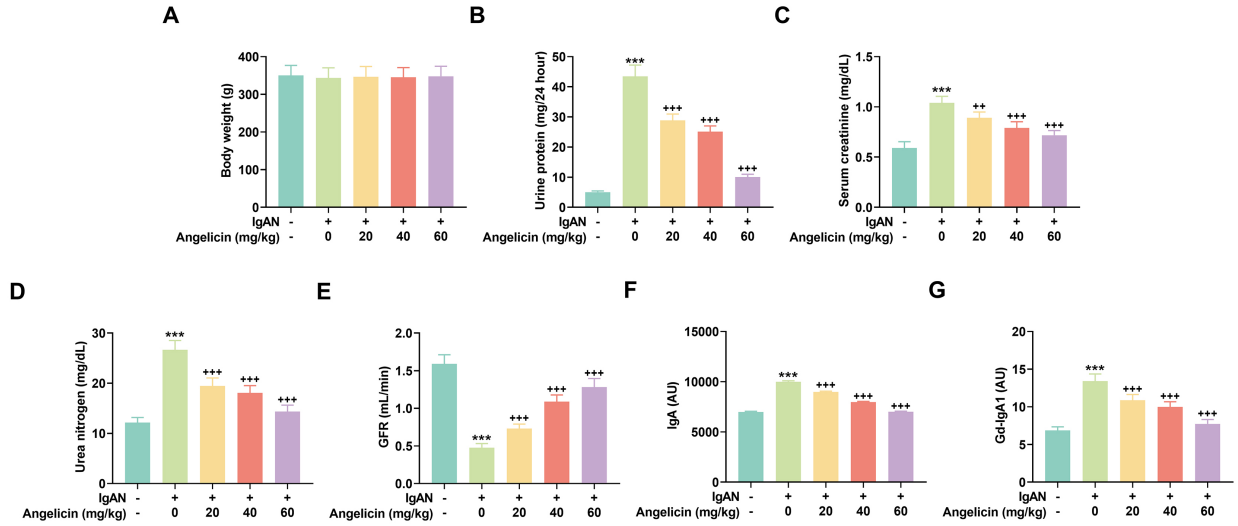

Fig. 1. Angelicin alleviates renal dysfunction. (A) Weight of rats in the control, IgAN, and angelicin-treated IgAN groups (20/40/60 mg/kg), respectively. (B–G) Urine protein (B), serum creatinine (C), urea nitrogen (D), glomerular filtration rates (GFR) (E), IgA (F) and glycosylated IgA1 (Gd-IgA1) (G) levels of rats in the control, IgAN, and angelicin-treated IgAN groups (20/40/60 mg/kg), respectively. *** $p < 0.001$ compared with control group; $^{++}$ $p < 0.01$, $^{+++}$ $p < 0.001$ compared with IgAN group. Data represent mean ± standard deviation (SD) ($n = 6$). Abbreviations: Gd-IgA1, glycosylated IgA1; IgAN, immunoglobulin A nephropathy.

that angelicin can suppress IgA deposition in the glomeruli. Higher concentrations of angelicin were more effective in reducing the red fluorescence ($p < 0.01$, Fig. 2A,B), indicating a dose-dependent reduction in IgA levels. H&E staining showed that the renal tissue structure of the control group rats was intact and well-preserved with normal glomerular size and no signs of swelling or degeneration in the renal tubules, nor infiltration or fibrosis in the interstitial area (Fig. 2C). In contrast, the IgAN group exhibited thickened glomeruli, renal interstitial edema, and extensive infiltration with inflammatory cells and fibrosis in the interstitial area (Fig. 2C). Treatment with 20 mg/kg angelicin resulted in a noticeable increase in kidney size, a darker red color, and minimal infiltration with inflammatory cells (Fig. 2C), indicating that angelicin can alleviate renal tissue damage. With increasing concentrations of angelicin, further alleviation of renal tissue damage was observed (Fig. 2C), demonstrating a dose-dependent mitigation of renal tissue damage.

TUNEL staining showed that cell apoptosis was significantly increased in the IgAN group (Fig. 2D), but angelicin treatment effectively reduced the number of apoptotic cells, with greater effects observed at higher dosages (Fig. 2D). Additionally, Masson trichrome staining (Fig. 2E) and immunohistochemical tests (Fig. 2F,G) further confirmed the potential of angelicin in ameliorating renal fibrosis. Compared to the control group, expression levels of α-SMA (Fig. 2F) and Col-IV (Fig. 2G) were significantly higher in the IgAN group, indicating severe renal fibrosis. However, angelicin significantly reduced the expression of these fibrosis markers, demonstrating dose-dependent antifibrotic effects (Fig. 2F,G).

Angelicin Suppresses Renal Inflammation and Fibrosis

Western blotting and ELISA experiments were performed to validate the results. Compared to the control group, the IgAN group featured significantly elevated levels of TGF-β1 (1.00 ± 0.14 vs. 2.80 ± 0.22, $p < 0.001$, F = 31.0088, DFn = 4, DFd = 10, Fig. 3A,B), Col-IV (1.00 ± 0.15 vs. 1.70 ± 0.02, $p < 0.001$, F = 213.7184, DFn = 4, DFd = 10, Fig. 3A,C), and fibronectin 1 (1.00 ± 0.16 vs. 2.04 ± 0.09, $p < 0.001$, F = 33.7845, DFn = 4, DFd = 10, Fig. 3A,D), but their expression levels were reduced after treatment with angelicin, especially at higher dosages ($p < 0.01$, Fig. 3A–D), indicating the anti-fibrotic properties of angelicin in kidney via a dose-dependent manner. Lastly, ELISA tests of inflammation markers IL-1β (40.04 ± 3.69 vs. 152.67 ± 11.45, $p < 0.001$, F = 235.7616, DFn = 4, DFd = 25, Fig. 3E), IL-6 (4.97 ± 0.43 vs. 23.35 ± 1.84, $p < 0.001$, F = 219.8924, DFn = 4, DFd = 25, Fig. 3F), and IL-18 (3.92 ± 0.34 vs. 33.75 ± 2.79, $p < 0.001$, F = 289.3059, DFn = 4, DFd = 25, Fig. 3G) also showed similar trends: Compared to the IgAN group, their angelicin-treated counterparts exhibited significantly reduced levels of these inflammation markers, with higher doses showing more significant effects ($p < 0.001$, Fig. 3E–G), further demonstrating the anti-inflammatory effects of angelicin in a dose-dependent manner. Collectively, these data indicate that angelicin significantly improves the pathological state of IgAN, alleviates kidney tissue damage and suppresses inflammatory responses, highlighting the therapeutic efficacy of angelicin for the clinical treatment of IgAN.

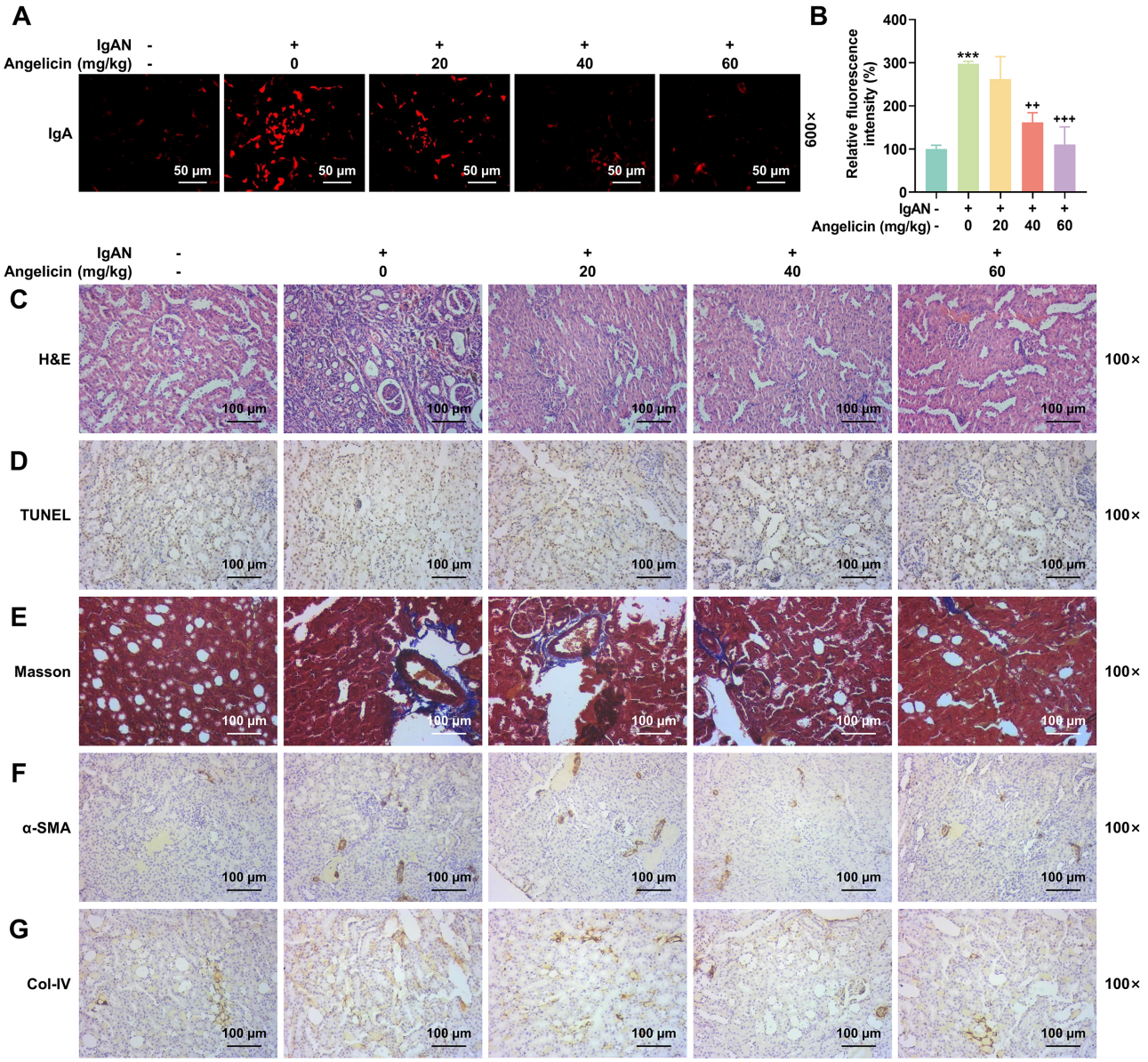

Fig. 2. Therapeutic effects of angelicin on IgAN. (A,B) Immunofluorescence staining results depicting varying levels of IgA deposition in the kidney tissues of rats in the control, IgAN, and angelicin-treated IgAN groups (20/40/60 mg/kg). The red fluorescence corresponds to the presence of IgA targeted by the Texas Red-conjugated antibody. The microscopy was conducted at a magnification of 600× and a scale of 50 μm. (C) Hematoxylin & Eosin (H&E) staining of rat kidney tissues from the control, IgAN, and angelicin-treated IgAN groups (20/40/60 mg/kg). (D) TUNEL staining of rat kidney tissue from the control, IgAN, and angelicin-treated IgAN groups (20/40/60 mg/kg). (E) Masson trichrome staining of rat kidney tissue from the control, IgAN, and angelicin-treated IgAN groups (20/40/60 mg/kg). (F,G) Immunohistochemical detection of α-smooth muscle actin (α-SMA) (F) and collagen type IV (Col-IV) (G) in the control, IgAN, and angelicin-treated IgAN groups (20/40/60 mg/kg). The brown parts in the images correspond to the positive staining of α-SMA (F) and Col-IV (G). *** $p < 0.001$ compared with control group; $^{++}$ $p < 0.01$, $^{+++}$ $p < 0.001$ compared with IgAN group. The microscopy was conducted at a magnification of 100× and a scale of 100 μm. Data represent means ± SD ($n = 3$).

Angelicin Mitigates IgAN by Mediating ESR1-FOS Signaling Pathway

To explore how angelicin alleviates IgAN, we employed a Western blot approach to investigate protein expression of ESR1, FOS, p-c-Jun and p-MAPK in the IgAN groups (Fig. 3H). We found that the protein levels of ESR1 (1.00 ± 0.11 vs. 1.81 ± 0.09, $p < 0.001$, F = 36.292, DFn = 4, DFd = 10, Fig. 3I), FOS (1.00 ± 0.17 vs. 2.10 ± 0.15, $p < 0.001$, F = 20.3164, DFn = 4, DFd = 10, Fig. 3J), p-c-Jun (0.64 ± 0.10 vs. 1.66 ± 0.17, $p < 0.001$, F = 41.925, DFn = 4, DFd = 10, Fig. 3K), and p-MAPK (1.03 ± 0.21 vs. 2.61 ± 0.36, $p < 0.001$, F = 18.9874, DFn = 4, DFd = 10, Fig. 3L)

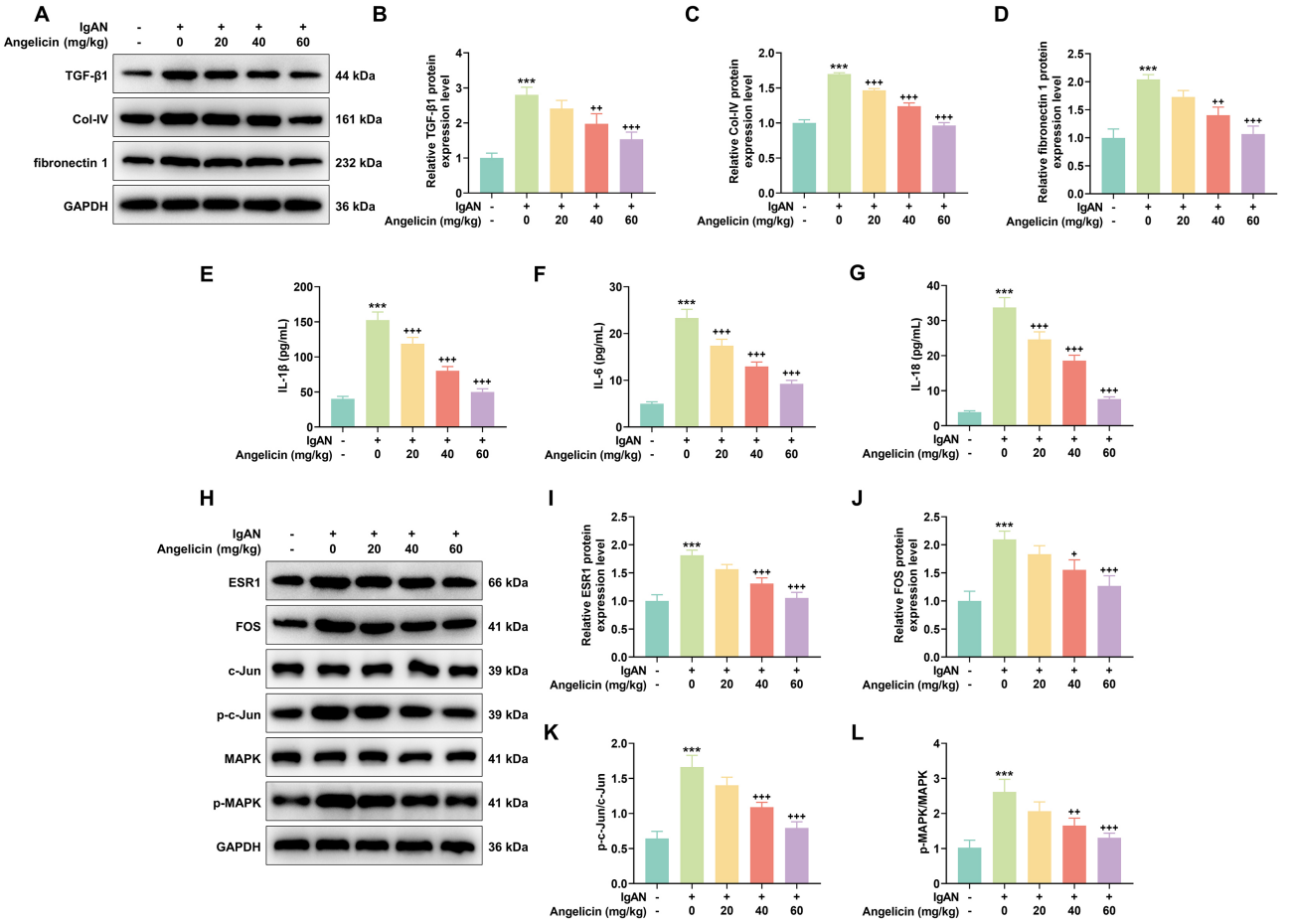

Fig. 3. Angelicin mitigates IgAN by mediating the ESR1-FOS signaling pathway. (A) Western blot-based detection of renal fibrosis in rats of the control, IgAN, and angelicin-treated IgAN groups (20/40/60 mg/kg). (B–D) Expression levels of TGF-β1 (B), collagen type IV (Col-IV) (C), and fibronectin1 (D) in the kidneys of rats in the control, IgAN, and angelicin-treated IgAN groups (20/40/60 mg/kg). (E–G) ELISA detection of serum levels of IL-1β (E), IL-6 (F) and IL-18 (G) in the rats of the control, IgAN, and angelicin-treated IgAN groups (20/40/60 mg/kg). (H) Western blot-based detection of ESR1, FOS, p-c-Jun and p-MAPK levels in rats of the control, IgAN, and angelicin-treated IgAN groups (20/40/60 mg/kg). (I–L) Expression levels of ESR1 (I), FOS (J), p-c-Jun (K) and p-MAPK (L) in the kidneys of rats in the control, IgAN, and angelicin-treated IgAN groups (20/40/60 mg/kg). *** $p < 0.001$ compared with control group; $^{+}$ $p < 0.05$, $^{++}$ $p < 0.01$, $^{+++}$ $p < 0.001$ compared with IgAN group. Data represent means $\pm$ SD (Western blot experiments, $n = 3$; ELISA experiments, $n = 6$). Abbreviations: ESR1, estrogen receptor 1; FOS, Fos proto-oncogene; IgAN, immunoglobulin A nephropathy; IL, Interleukin; TGF-β1, transforming growth factor beta 1.

were elevated, which are linked to active cell signaling in the pathological state of IgAN. Treatment with 40 mg/kg angelicin significantly reduced the expression of these proteins, and further reductions were observed as the concentration of angelicin increased ($p < 0.05$, Fig. 3I–L). These results suggest that angelicin effectively inhibits inflammatory and fibrotic pathways associated with IgAN, and its action is clearly dose-dependent. Angelicin significantly influences renal pathological responses by modulating the key signaling molecules—a potential molecular mechanism underlying its therapeutic efficacy in the context of IgAN.

Discussion

The findings from this study offer significant insights into the therapeutic potential of angelicin in IgAN. As a major contributor to glomerulonephritis, IgAN is characterized by the deposition of IgA in the glomerular mesangium, leading to progressive renal impairment [21,22]. Despite advancements in medical treatments, the management of IgAN remains challenging due to its complex pathogenesis and variable clinical outcomes. Our research contributes to understanding the role of angelicin in modern medical applications, particularly through the modulation of specific molecular pathways involved in the disease process.

The discussion of angelicin's efficacy in treating IgAN through its impact on renal fibrosis and inflammation, based on modulation of the ESR1-FOS pathway, is pivotal. Our study indicates that angelicin in varying dosages did not significantly impact the body weight of the IgAN rats, compared to their untreated counterparts. This stability in body weight, despite the presence of kidney disease and the administration of different doses of angelicin, supports its safety profile, suggesting minimal systemic toxicity at therapeutic doses. This observation is crucial as safety concerns are a primary barrier to the clinical translation of many new therapeutic agents.

Prior studies have reported that angelicin can be used to treat fibrosis [10,23], but its role in IgAN remains largely unexplored. Our data extend these findings by identifying angelicin's effectiveness in IgAN rats. The therapeutic benefits of angelicin are reflected by its significant impact on biochemical markers of renal function in IgAN rats. For instance, treatment with angelicin resulted in decreased levels of urine protein, serum creatinine, and urea nitrogen, alongside an improvement in glomerular filtration rates, indicating a reversal of renal dysfunction. It has been reported that the expression of α-SMA contributes directly to experimental hepatic fibrogenesis and indirectly to fibrogenesis in human chronic liver disease [24]. The reduced expression of α-SMA and Col-IV, which are crucial markers of fibrosis, further confirms the antifibrotic action of angelicin. These changes not only highlight the therapeutic potential of angelicin in reducing kidney fibrosis but also underscore its role in improving the overall kidney function, critical for delaying the progression of IgAN.

In post-traumatic osteoarthritis, angelicin alleviates disease progression by suppressing IL-1β and tumor necrosis factor alpha (TNF-α) secretion while promoting macrophage polarization toward the M2 phenotype [25]. Similarly, in our IgAN model, angelicin significantly reduced renal levels of IL-1β, IL-6, and IL-18—cytokines central to mesangial inflammation and fibrosis. This reduction correlates with the observed decreases in ESR1 and FOS protein levels. Although ESR1 is best characterized in hormone-dependent cancers such as breast cancer [26,27], its role in renal fibrosis remains underexplored. Our finding of ESR1 upregulation in the treatment model of IgAN suggests a potential regulatory effect in kidney disease; inhibiting ESR1 may reduce fibrosis and thus treat IgAN. The dose-responsive nature of these effects suggests that angelicin interacts dynamically with its molecular targets, offering insights into how therapeutic dosing could be optimized in clinical settings. By effectively downregulating these key transcription factors, angelicin not only addresses the inflammatory component of IgAN but also helps in curtailing the fibrotic processes that these proteins can exacerbate. Because of the complex underlying mechanisms of the disease, monotherapy is unlikely to be effective for all IgAN patients. Compared to emerging complement-targeted therapies [7], angelicin offers a distinct yet complementary mechanism. While complement inhibitors primarily block downstream inflammatory damage, angelicin targets upstream signaling hubs (ESR1-FOS) that regulate both fibrosis and cytokine production (e.g., IL-6, IL-1β). This dual action may explain its broader efficacy in our model, where we observed reductions in both inflammatory markers and fibrosis.

Furthermore, the observation that higher doses resulted in more pronounced improvements suggests that angelicin interacts with its molecular targets in a dose-dependent manner, which is crucial for defining optimal dosing strategies in future clinical trials. Understanding the dose-response relationship is essential for maximizing therapeutic efficacy while minimizing potential risks. While we observed ESR1-FOS suppression, the upstream triggers remain unclear. Given that TGF-β1 can inhibit ESR1 transcription [28] and is also a core driver of renal fibrosis, it may promote fibrotic progression by inhibiting ESR1 expression [29,30]. In summary, the broad spectrum of angelicin's impact, from reducing fibrotic markers to mitigating inflammation via modulation of the ESR1-FOS pathway, demonstrates its comprehensive therapeutic potential. Taken together, this multifaceted compound offers an effective solution for managing IgAN, but further research into angelicin's clinical applications as part of targeted therapies in managing chronic kidney diseases, including IgAN, is warranted.

Several limitations of this study should be highlighted. Firstly, the therapeutic effects of angelicin that are evident in our rat model cannot be extrapolated to the human IgAN context at the current stage. Specifically, nuances in metabolism, immune response, and chronicity of disease modeled in animals are not fully replicable in humans. Future studies should focus on clinical trials to validate these promising results in human subjects and to explore the pharmacokinetics, optimal dosing, and long-term safety of angelicin in the treatment of IgAN. Secondly, a larger sample size can improve the reliability of this experiment. Thirdly, the bioinformatics analyses were unable to predict a direct physical interaction between CKAP2L and ADORA2A, suggesting a mediating relationship involving other currently uncharacterized factors, which represents an important direction for future work. Finally, a lack of knockout/overexpression experiments prevents causal attribution to ESR1/FOS. Future *in vitro* or *in vivo* functional validation experiments (e.g., ESR1 knockout or FOS overexpression) will be needed to confirm their involvement in the mechanism of action of angelicin.

Conclusions

In conclusion, our study contributes to the growing body of evidence that supports the adoption of angelicin in the armada of therapies against chronic diseases, such as

IgAN. By elucidating the specific actions of angelicin on key molecular pathways involved in renal pathology, we lay a foundation for further research on the potential clinical applications of angelicin, as part of future investigative endeavors to develop more effective and targeted therapies for managing IgAN.

Availability of Data and Materials

The datasets used and/or analyzed during the current study are available from the corresponding author upon reasonable request.

Author Contributions

Substantial contributions to conception and design: HJF. Data acquisition, data analysis and interpretation: LZ, XCX, TTZ, SQL, CJ. Drafting the article or critically revising it for important intellectual content: All authors. Final approval of the version to be published: All authors. Agreement to be accountable for all aspects of the work in ensuring that questions related to the accuracy or integrity of the work are appropriately investigated and resolved: All authors.

Ethics Approval and Consent to Participate

All animal experiments were conducted in compliance with institutional guidelines for the care and use of laboratory animals and were approved by the Laboratory Animal Welfare and Ethics Committee of Jinhua Municipal Central Hospital (No. AL-JHYY202401). The study design, experimental procedures, and reporting of results follow the ARRIVE guidelines to ensure high-quality and reproducible animal research.

Acknowledgment

Not applicable.

Funding

This work was supported by Zhejiang Province Medical and Health Science and Technology Project in 2025 (No. 2025KY1741).

Conflict of Interest

The authors declare no conflict of interest.

References

[1] Ma S, Zhao M, Chang M, Shi X, Shi Y, Zhang Y. Effects and mechanisms of Chinese herbal medicine on IgA nephropathy. Phytomedicine: International Journal of Phytotherapy and Phytopharmacology. 2023; 117: 154913. https://doi.org/10.1016/j.phymed.2023.154913.

[2] Ellison B, Cader R, Willcocks L. Advances in primary glomerulonephritis. British Journal of Hospital Medicine (London, England: 2005). 2024; 85: 1–11. https://doi.org/10.12968/hmed.2024.0044.

[3] Nihei Y, Suzuki H, Suzuki Y. Current understanding of IgA antibodies in the pathogenesis of IgA nephropathy. Frontiers in Immunology. 2023; 14: 1165394. https://doi.org/10.3389/fimmu.2023.1165394.

[4] Xu B, Bao Q, Shen W, Hong Q. Clinicopathological Features of Membranous Nephropathy Complicated by IgA Nephropathy: A Retrospective Analysis of Seven Cases. British Journal of Hospital Medicine (London, England: 2005). 2024; 85: 1–13. https://doi.org/10.12968/hmed.2024.0338.

[5] Novak J, Barratt J, Julian BA, Renfrow MB. Aberrant Glycosylation of the IgA1 Molecule in IgA Nephropathy. Seminars in Nephrology. 2018; 38: 461–476. https://doi.org/10.1016/j.semnephrol.2018.05.016.

[6] Tesař V, Radhakrishnan J, Charu V, Barratt J. Challenges in IgA Nephropathy Management: An Era of Complement Inhibition. Kidney International Reports. 2023; 8: 1730–1740. https://doi.org/10.1016/j.ekir.2023.06.010.

[7] Caravaca-Fontán F, Gutiérrez E, Sevillano ÁM, Praga M. Targeting complement in IgA nephropathy. Clinical Kidney Journal. 2023; 16: ii28–ii39. https://doi.org/10.1093/ckj/sfad198.

[8] Lescoat A, Lelong M, Jeljeli M, Piquet-Pellorce C, Morzadec C, Ballerie A, *et al*. Combined anti-fibrotic and anti-inflammatory properties of JAK-inhibitors on macrophages in vitro and in vivo: Perspectives for scleroderma-associated interstitial lung disease. Biochemical Pharmacology. 2020; 178: 114103. https://doi.org/10.1016/j.bcp.2020.114103.

[9] Bakery HH, Allam GA, Abuelsaad ASA, Abdel-Latif M, Elkenawy AE, Khalil RG. Anti-inflammatory, antioxidant, anti-fibrotic and schistosomicidal properties of plumbagin in murine schistosomiasis. Parasite Immunology. 2022; 44: e12945. https://doi.org/10.1111/pim.12945.

[10] Carbone A, Montalbano A, Spanò V, Musante I, Galietta LJV, Barraja P. Furocoumarins as multi-target agents in the treatment of cystic fibrosis. European Journal of Medicinal Chemistry. 2019; 180: 283–290. https://doi.org/10.1016/j.ejmech.2019.07.025.

[11] Mirfazeli ES, Marashi SA, Kalantari S. In silico prediction of specific pathways that regulate mesangial cell proliferation in IgA nephropathy. Medical Hypotheses. 2016; 97: 38–45. https://doi.org/10.1016/j.mehy.2016.10.014.

[12] Xie L, Cheng Y, Du W, Fu L, Wei Z, Guan Y, *et al*. Activation of GPER1 in macrophages ameliorates UUO-induced renal fibrosis. Cell Death & Disease. 2023; 14: 818. https://doi.org/10.1038/s41419-023-06338-2.

[13] Cui Y, Chen C, Tang Z, Yuan W, Yue K, Cui P, *et al*. TREM2 deficiency aggravates renal injury by promoting macrophage apoptosis and polarization via the JAK-STAT pathway in mice. Cell Death & Disease. 2024; 15: 401. https://doi.org/10.1038/s41419-024-06756-w.

[14] Zhao T, Sun Z, Lai X, Lu H, Liu L, Li S, *et al*. Tamoxifen exerts anti-peritoneal fibrosis effects by inhibiting H19-activated VEGFA transcription. Journal of Translational Medicine. 2023; 21: 614. https://doi.org/10.1186/s12967-023-04470-3.

[15] Zhang Y, Wang Q, Wang ZX, Bi YN, Yuan XM, Song L, *et al*. A Study of NMR-Based Hepatic and Serum Metabolomics in a Liver Injury Sprague-Dawley Rat Model Induced by Psoralen. Chemical Research in Toxicology. 2018; 31: 852–860. https://doi.org/10.1021/acs.chemrestox.8b00082.

[16] Li X, Yu C, Hu Y, Xia X, Liao Y, Zhang J, *et al*. New Application of Psoralen and Angelicin on Periodontitis With Antibacterial, Anti-inflammatory, and Osteogenesis Effects. Frontiers in Cellular and Infection Microbiology. 2018; 8: 178. https://doi.org/10.3389/fcimb.2018.00178.

[17] Liu W, Shi L, Wan Q, Wu Y, Huang D, Ou J, *et al*. Huangqi Guizhi Wuwu Decoction attenuates Podocyte cytoskeletal protein damage in IgA nephropathy rats by regulating AT1R/Nephrin/c-Abl pathway. Biomedicine & Pharmacotherapy = Biomedecine & Pharmacotherapie. 2021; 142: 111907. https://doi.org/10.1016/j.biopha.2021.111907.

[18] Alshaman R, Truong L, Oyekan A. Role of mechanistic target of rapamycin (mTOR) in renal function and ischaemia-reperfusion induced kidney injury. Clinical and Experimental Pharmacology & Physiology. 2016; 43: 1087–1096. https://doi.org/10.1111/1440-1681.12648.

[19] Yasutake J, Suzuki Y, Suzuki H, Hiura N, Yanagawa H, Makita Y, *et al*. Novel lectin-independent approach to detect galactose-deficient IgA1 in IgA nephropathy. Nephrology, Dialysis, Transplantation: Official Publication of the European Dialysis and Transplant Association - European Renal Association. 2015; 30: 1315–1321. https://doi.org/10.1093/ndt/gfv221.

[20] Makita Y, Suzuki H, Kano T, Takahata A, Julian BA, Novak J, *et al*. TLR9 activation induces aberrant IgA glycosylation via APRIL- and IL-6-mediated pathways in IgA nephropathy. Kidney International. 2020; 97: 340–349. https://doi.org/10.1016/j.kint.2019.08.022.

[21] Selvaskandan H, Gonzalez-Martin G, Barratt J, Cheung CK. IgA nephropathy: an overview of drug treatments in clinical trials. Expert Opinion on Investigational Drugs. 2022; 31: 1321–1338. https://doi.org/10.1080/13543784.2022.2160315.

[22] Tang YY, Liu T, Wu X, Zhang YT, Wei LB, Gao YC, *et al*. The combined analysis of metabolomics and transcriptomics revealed the metabolic changes of kidney tissue in mice with IgA nephropathy. Genomics. 2025; 117: 111076. https://doi.org/10.1016/j.ygeno.2025.111076.

[23] Lampronti I, Manzione MG, Sacchetti G, Ferrari D, Spisani S, Bezzerri V, *et al*. Differential Effects of Angelicin Analogues on NF-κB Activity and IL-8 Gene Expression in Cystic Fibrosis IB3-1 Cells. Mediators of Inflammation. 2017; 2017: 2389487. https://doi.org/10.1155/2017/2389487.

[24] Mostafa ME, Shaaban AA, Salem HA. Dimethylfumarate ameliorates hepatic injury and fibrosis induced by carbon tetrachloride. Chemico-biological Interactions. 2019; 302: 53–60. https://doi.org/10.1016/j.cbi.2019.01.029.

[25] Tian Z, Zeng F, Zhao C, Dong S. Angelicin Alleviates Post-Trauma Osteoarthritis Progression by Regulating Macrophage Polarization via STAT3 Signaling Pathway. Frontiers in Pharmacology. 2021; 12: 669213. https://doi.org/10.3389/fphar.2021.669213.

[26] Brett JO, Spring LM, Bardia A, Wander SA. ESR1 mutation as an emerging clinical biomarker in metastatic hormone receptor-positive breast cancer. Breast Cancer Research: BCR. 2021; 23: 85. https://doi.org/10.1186/s13058-021-01462-3.

[27] Venetis K, Pepe F, Pescia C, Cursano G, Criscitiello C, Frascarelli C, *et al*. ESR1 mutations in HR+/HER2-metastatic breast cancer: Enhancing the accuracy of ctDNA testing. Cancer Treatment Reviews. 2023; 121: 102642. https://doi.org/10.1016/j.ctrv.2023.102642.

[28] Lung DK, Reese RM, Alarid ET. Intrinsic and Extrinsic Factors Governing the Transcriptional Regulation of ESR1. Hormones & Cancer. 2020; 11: 129–147. https://doi.org/10.1007/s12672-020-00388-0.

[29] Higgins CE, Tang J, Mian BM, Higgins SP, Gifford CC, Conti DJ, *et al*. TGF-β1-p53 cooperativity regulates a profibrotic genomic program in the kidney: molecular mechanisms and clinical implications. FASEB Journal: Official Publication of the Federation of American Societies for Experimental Biology. 2019; 33: 10596–10606. https://doi.org/10.1096/fj.201900943R.

[30] Ruby M, Gifford CC, Pandey R, Raj VS, Sabbisetti VS, Ajay AK. Autophagy as a Therapeutic Target for Chronic Kidney Disease and the Roles of TGF-β1 in Autophagy and Kidney Fibrosis. Cells. 2023; 12: 412. https://doi.org/10.3390/cells12030412.